Thermal enhancement of the oxidation layer of micron-sized aluminum powder and its anti-oxidation performance

Yang Liu

The Civil-Military Integration Institute, China Center for Information Industry Development, Beijing 100091, China
liuyang@ccidthinktank.com

Abstract: Micron-sized aluminum powder, with its typical core-shell structure, exhibits oxidation behavior upon slow heating in an oxidative atmosphere that is related to the particle size of the aluminum powder. A particle size-dependent thermal response mechanism for micron-sized aluminum powder is established: a "shell-breaking eruption" thermal response mechanism. The oxide layer is thermally enhanced, and the anti-oxidation reaction behavior mechanism of the enhanced samples is studied. Aluminum powder samples, heated slowly to specific temperatures to obtain changes in the oxide layer structure, are analyzed using a thermal analyzer to compare the slow heating response behavior of aluminum powder before and after the oxidation layer changes. It was found that after thermal enhancement of the aluminum powder oxidation layer, which changed from amorphous to γ-phase and whose thickness increased to twice the original thickness, the slow oxidation process of micron-sized aluminum powder was inhibited, and the aluminum powder was completely deactivated in the slow heating response.

Keywords: micron-sized aluminum powder; core-shell structure; oxidation layer enhancement; thermal response

1. Introduction

Aluminum powder, as an additive component in energetic systems [1-3], especially in propellants [4,5] and thermite [6], significantly improves the performance of energetic systems, such as controlling burn rate, reducing engine vibration, etc. [7-10][4, 5]. The particle size and activity of aluminum powder significantly impact the energy release of energetic systems [6, 7]. Clarifying the thermal response mechanism of aluminum powder under different conditions can guide its application in energetic systems. Studies involving slow heating experiments, which unfold the thermal response process of aluminum powder over time, have always been a focus of researchers [11-18]. Cheng Zhipeng, Zeng Liang, and others have conducted related studies on the oxidation reaction of aluminum powder under slow heating conditions [21,22], however, research on the impact of the oxide layer structure on the thermal response process, and the differences in the thermal response process caused by structural changes in the oxide layer under temperature influence, remains insufficient.

Nano aluminum powder in practical applications contains significantly less active component than micron aluminum powder and is prone to deactivation during the blending process in energetic systems. Therefore, micron-scale aluminum powder holds a more important position in energetic systems. Micron aluminum powder is a typical core-shell structure, consisting of an internal aluminum core and an outer uniformly coated amorphous alumina layer. The alumina passivation layer can protect the active aluminum from further oxidation with the external environment under certain conditions. However, the high melting and boiling points and high density of the oxide layer also make the thermal response mechanism of aluminum powder complex and difficult to directly analyze and observe.

Alumina exists in various crystal forms, for instance, the coating layer of micron aluminum powder in its natural state is amorphous alumina, and other common crystal forms include γ, δ, θ. These types of alumina are transition states (metastable) and typically have some activity. They will eventually transform into α-phase at high temperatures, the most stable form. The material undergoes γ (450℃) → δ (850℃) → θ (1100℃) → α (≥1200℃) alumina changes during the transformation from amorphous to stable α-alumina [8-12]. γ-Alumina has a spinel structure with cation deficiency, composed of cubic close-packed oxygen anions layers, with aluminum cations in octahedral and tetrahedral positions; α-alumina has a corundum

structure, composed of hexagonally packed oxygen anion layers with aluminum in only octahedral positions [12]. The oxidation layer of micron aluminum powder is an important factor affecting its activity. Studying the thermal response mechanism of aluminum powder with different oxide layer structures can provide references for the active protection of energetic materials and lay a theoretical foundation for the application of aluminum powder in energetic systems [24].

This paper focuses on the changes in the oxidation layer of micron aluminum powder during the slow heating process. By controlling the temperature program, the structure and strength of the oxide layer are processed. The thermal response processes of aluminum powder before and after the enhancement of the oxide layer are analyzed and compared, and the mechanism of the thermal response process of micron aluminum powder particle size and oxide layer enhancement is established.

2. Experimental Section

2.1. Experimental Samples and Instruments

The micron aluminum powder used in the experiment, prepared by the spray method and sieved through an air jet sieve machine, was supplied by Anshan Iron and Steel Industrial Micron Aluminum Powder Co., Ltd. Before the heating experiments, the micron aluminum powder was dried in a vacuum oven at 35°C for 24 hours to eliminate moisture and other volatile substances that might interfere with the experimental results.

A NETZSCH STA449F3 thermogravimetric analyzer (TG-DSC) was used to study the slow heating of the samples. TG-DSC can accurately measure the mass and heat changes of the samples during heating in different atmospheric environments, and by controlling the heating program, the physical changes and chemical reactions of the materials can be precisely studied.

2.2. Experimental Procedure

The heating rate of the instrument was set to 20°C/min, with an effective heating temperature range from 300°C to 1450°C. The atmospheric environment included oxidizing oxygen and inert argon gases, with a constant gas flow rate of 1.2L/h, ensuring complete reaction of the gas with the aluminum powder samples while maintaining a constant reaction environment pressure to some extent. Pre-treated aluminum powder samples were weighed in a dry environment, with each experiment controlling the sample mass to 3mg±0.3mg, evenly placed at the bottom of the alumina crucible. For accuracy and repeatability, each set of experiments was repeated three times.

2.3. Preparation of Oxidation Layer Enhanced Samples

Using the TG-DSC analyzer, micron aluminum powder was slowly heated in an oxygen environment. Based on existing research, at 450°C, the alumina begins to undergo a crystal transformation. Three temperatures, 450°C, 550°C, and 650°C, were selected for the treatment of the oxide layer, and subsequent experimental temperature settings were determined based on preliminary results. After heating to the specific temperature in an oxygen atmosphere, the cooling program was initiated, and the atmospheric environment was switched to argon gas purging until room temperature was reached. The aluminum powder samples before and after treatment were characterized, and samples with changes in the phase and structure of alumina at specific temperatures were selected for comparative studies of slow heating response.

3. Experimental Results and Analysis

3.1. Morphological Characteristics of Aluminum Powder

3.1.1. Particle Size and Composition Characterization

A Malvern Mastersizer 2000 laser particle size analyzer was used to characterize the particle size distribution of the samples, as shown in Figure 1. The composition of the samples was characterized using a German ELEMENT GD glow discharge mass spectrometer. The active aluminum content was determined using the standard gas volumetric method. The four samples, along with their corresponding median particle

size, impurity content, and active aluminum content, are listed in Table 1. The aluminum powder samples had a high active content and low impurity content, reasonably neglecting the impact of impurities in subsequent hypothetical calculations.

Table 1: Diameter, Active Aluminum, and the Content of Aluminum Powders

Sample	D_{50}	Active aluminum	Content of impurity(%)			
			Cu	Fe	Si	H_2O
Al#1	2.51μm	98.16%	0.0004	0.0067	0.0024	0.0083
Al#2	5.24μm	98.30%	0.0004	0.0034	0.0070	0.0081
Al#3	13.35μm	98.67%	0.0004	0.0028	0.0068	0.0080
Al#4	24.02μm	98.80%	0.0004	0.0054	0.0087	0.0081

Statistical analysis using the Kolmogorov-Smirnov test showed that the particle size distribution of micron aluminum powder prepared by the spray method follows a log-normal distribution, with a high degree of fitting to formula 1. In the formula, x is the sample diameter (um), and y0, μ, σ, A are variables that can be obtained through fitting.

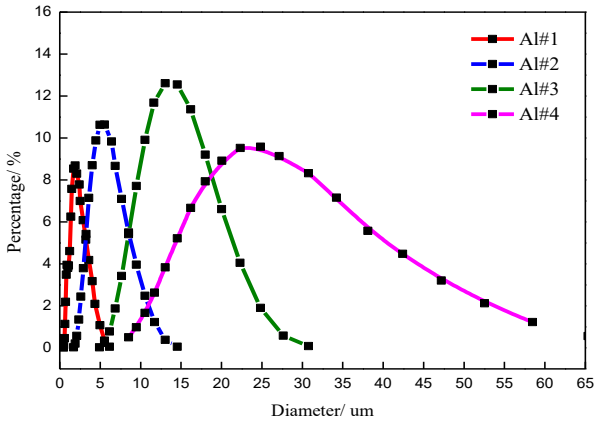

Figure 1: Size Distribution and Fitting Curves of Aluminum Powder

$$f(x) = y_0 + \frac{A}{\sqrt{2\pi}\sigma x} \cdot e^{-\frac{(\ln x - \mu)^2}{2\sigma^2}} \quad (1)$$

3.1.2. SEM Characterization

The morphological characteristics of the micron aluminum powder were characterized using a Hitachi S2700 Scanning Electron Microscope (SEM). The SEM images, as shown in Figure 2, indicate that all four aluminum powder samples have good sphericity, complete surface alumina layers, no agglomeration, and a relatively uniform particle size distribution.

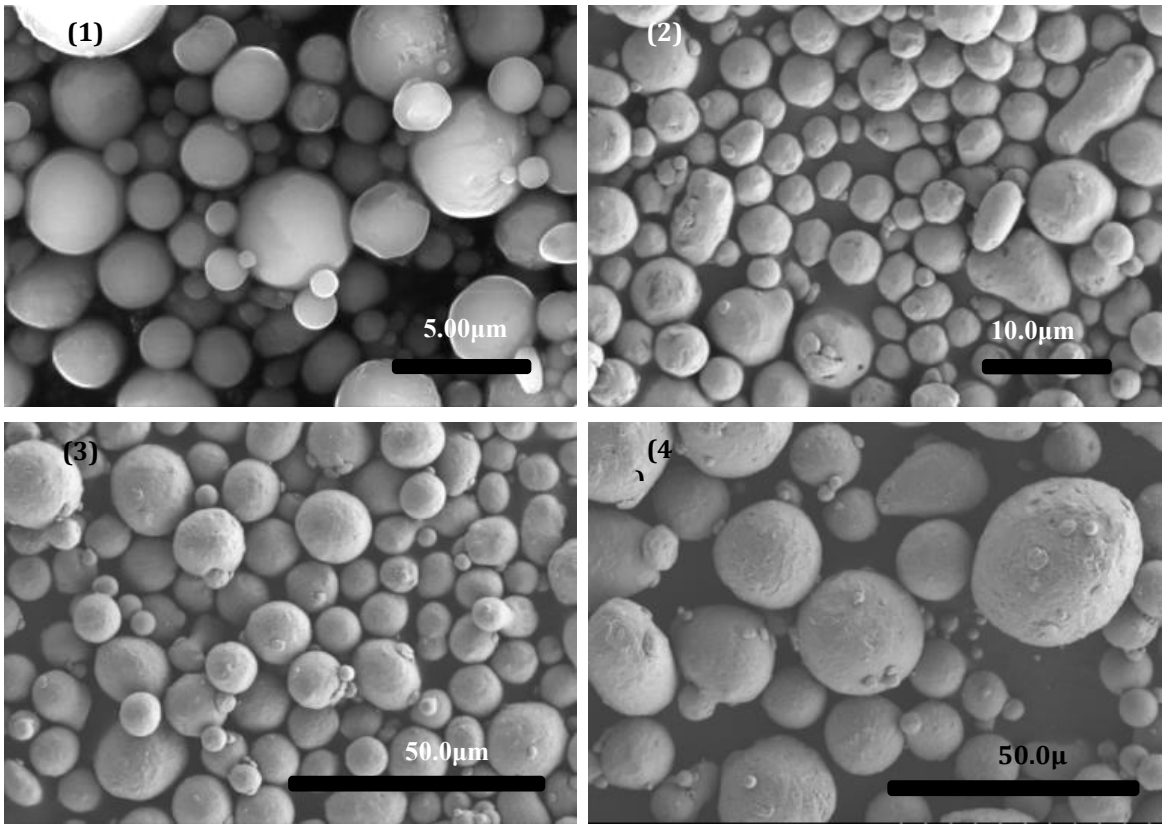

Figure 2: SEM Images of Aluminum Powders
(1) Al#1; (2) Al#2; (3) Al#3; (4) Al#4

3.1.3. XRD Characterization

The crystal structure of the samples was characterized using a Philips PW1710 powder diffractometer. The results, shown in Figure 3, take Al#2 as an example: the 2θ values are 38.47°, corresponding to Al (111); 44.719°, corresponding to Al (200); 65.095°, corresponding to Al (220); 78.226°, corresponding to Al (311). The crystal structure of aluminum is well-formed, with the outer alumina layer being amorphous.

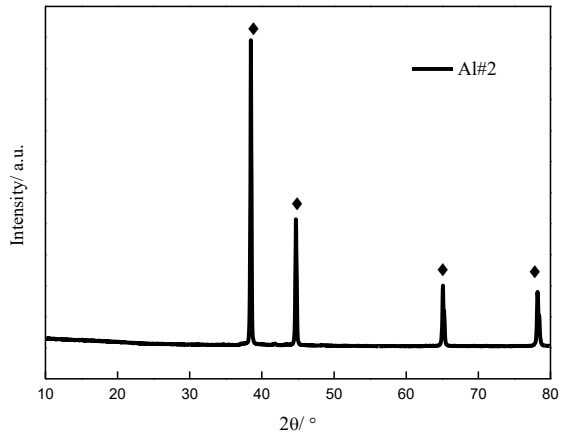

Figure 3: XRD Pattern of Al#2 Sample

3.2. Oxidation Layer Enhanced Aluminum Powder

Based on the phase transition temperature of alumina, aluminum powder was heated to 450°C, 550°C, and 650°C in an oxygen environment, keeping the heating temperature below the melting point of aluminum. Taking Al#2 as an example, the TG-DSC curve is shown in Figure 4. The experiments show that at 450°C and 550°C, there are no changes in the TG-DSC curve of the aluminum powder. At 650°C, a slight increase in weight and heat release occurs. Intermediate products collected were characterized using XRD, revealing the transformation of alumina from amorphous to γ-Al2O3. The weight increase indicates partial oxidation of active aluminum with the environmental atmosphere.

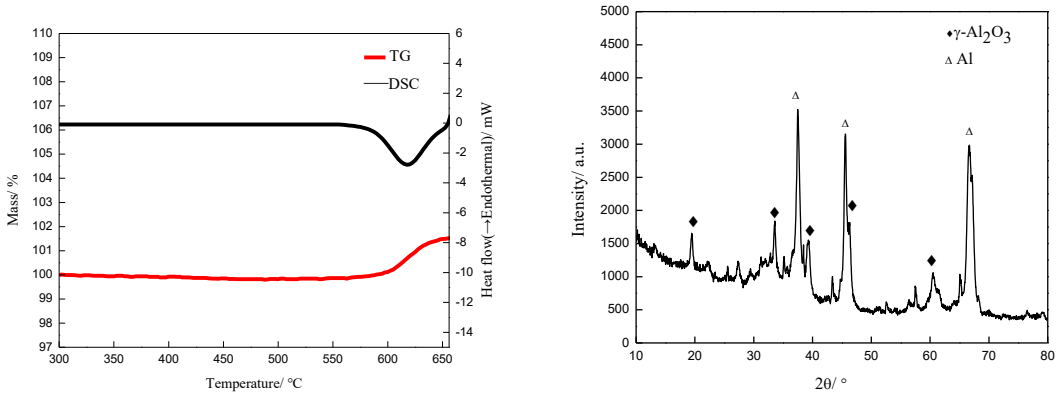

Figure 4: TG-DSC Curve of Al#2 and XRD Pattern of Al#2 Heated to 650°C

3.3. Thermal Response of Original Micron Aluminum Powder

3.3.1. Thermal Response Behavior of Micron Aluminum Powder

The TG-DSC curve of the original micron aluminum powder slowly heated in an oxygen environment, as shown in Figure 5, has three stages of weight increase: the first stage starts at 600°C (see magnified part), corresponding to exothermic peak 1, with the weight increase decreasing as the particle size increases, and 667°C being the melting endothermic point of aluminum; the second stage of weight increase starts from 850°C, continues to 1050°C, with the maximum weight increase rate at 950°C, corresponding to exothermic peak 3, the main reaction stage; the third stage starts from 1200°C, with the sample continuing to react, the rate of weight increase decreases, and the final product's mass increase at 1450°C decreases as the particle size increases.

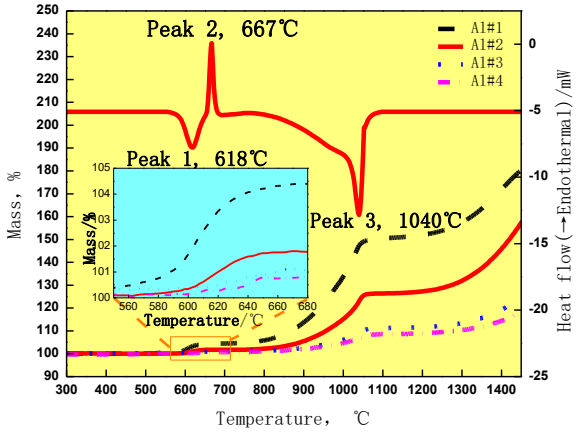

Figure 5: TG Curves from Al#1 to Al#4 and DSC Curve of Al#2

The weight increase of samples with different particle sizes at different temperatures is shown in Table 2. In an oxygen environment, the reaction of aluminum powder with the environment is shown in Equation (2). By mass increase and chemical equations, the percentage of oxidized active aluminum can be calculated.

$$Al + 4O2 = 2Al2O3 \quad (2)$$

Table 2: The Mass Increase of Aluminum Powders at Different Temperatures

Sample	Mass/ %	650℃/ %	950℃/ %	1200℃/ %	1450℃/ %
Al#1	100%	104.4578	121.6631	151.4992	179.9256
Al#2		102.0223	109.3915	127.3033	157.3223
Al#3		101.6922	103.9968	111.6802	124.8737
Al#4		101.3973	103.1937	109.0128	118.4680

3.3.2. Characterization of Intermediate Products

To further clarify the slow heating process of aluminum powder, the experiment was stopped at the temperatures shown in Table 2 and cooled to room temperature in an inert atmosphere. The collected products were characterized. According to Figures 6 and 7, the SEM photos and XRD patterns of Al#2 intermediate products show: at 620°C, the aluminum particles still maintain a complete spherical state; at temperatures above the melting point of aluminum, i.e., the beginning of the second stage of weight increase, the sample shows a hollow shell structure and broken alumina fragments; continued heating to 1350°C still reveals a hollow spherical shell structure with some deformation, indicating that unreacted molten active aluminum continues to overflow from the alumina coating and react with oxygen to form alumina.

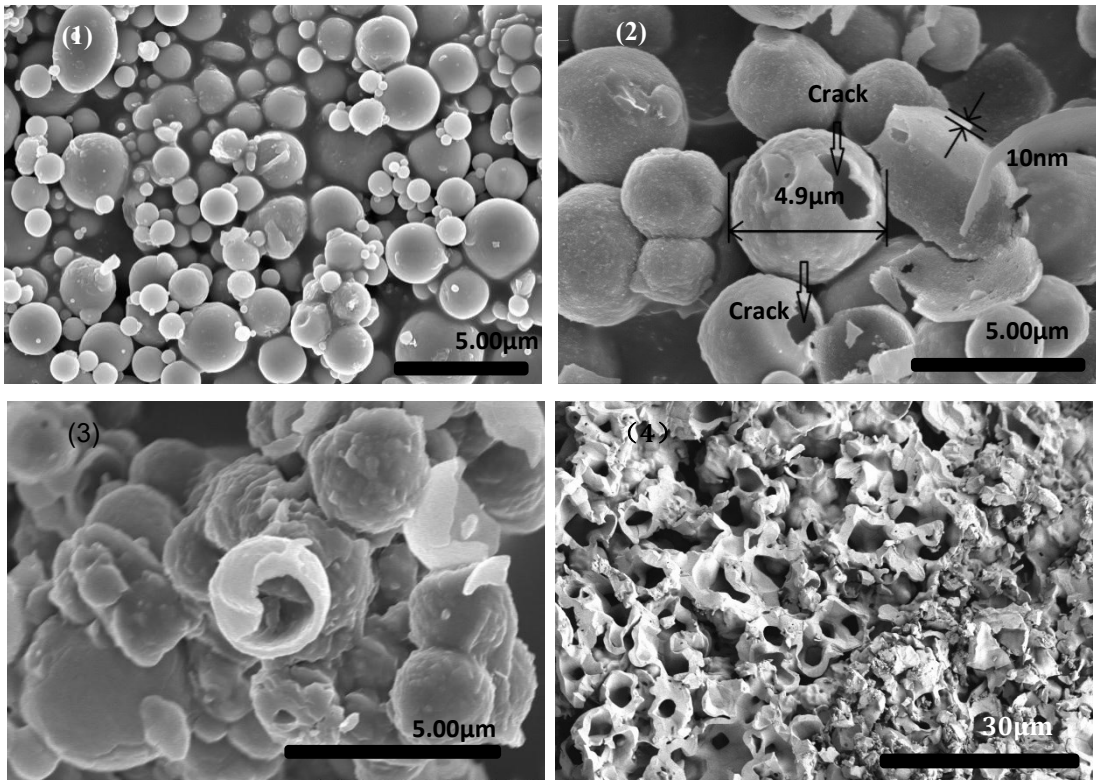

Figure 6: SEM Images of Al#2 Intermediate Products at Different Temperatures
(1) 650°C; (2) 950°C; (3) 1200°C; (4) 1450°C

At 650°C, the alumina shell transforms from the initial amorphous state to γ-Al2O3; at 950°C, alumina shows various crystal forms, including γ-Al2O3, θ-Al2O3, α-Al2O3. At this temperature, the sample is at the end of the first stage of weight increase and the beginning of the second stage, with the reaction temperature gradually increasing and the reaction state being relatively complex, and the oxide layer not

being a single phase; above 1200°C, the reaction rate decreases and slowly increases with temperature. The oxidation reaction continues, aluminum continues to oxidize, and at the same time, the phase of alumina continues to transform, eventually forming stable α-Al2O3, with the crystal structure being essentially the same as the final product.

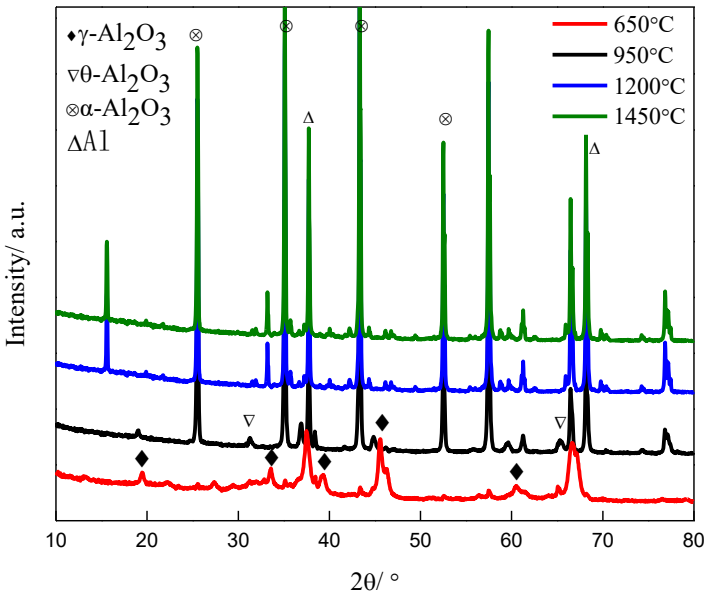

Figure 7: XRD Patterns of Al#2 Intermediate Products at Different Temperatures
(1) 650°C; (2) 950°C; (3) 1200°C; (4) 1450°C

3.4. Thermal Response of Samples after Oxidation Layer Treatment

After the oxidation layer was thermally treated by heating to 650°C, the sample codes are Al#1* to Al#4*. By comparing the slow thermal response of samples before and after the oxidation layer thermal treatment, the results are shown in Figure 8. Taking Al#2 as an example, the thermal response process of Al#2* no longer has the 1, 2, 3 stages of weight increase, and the corresponding exothermic peaks disappear, only showing the corresponding melting endothermic process at 667°C.

Comparisons of samples in different atmospheres reveal that after the oxidation layer was heated to 650°C and enhanced, the reaction of all samples in the oxidation environment was inhibited. As shown in Figure 9, taking Al#2 as an example, Al#2* in oxygen and carbon dioxide environments compared to the original sample's thermal responsiveness in an inert environment is consistent, with the insignificant weight increase process being caused by the oxidation of sub-micron or nano-sized aluminum powder in the sample.

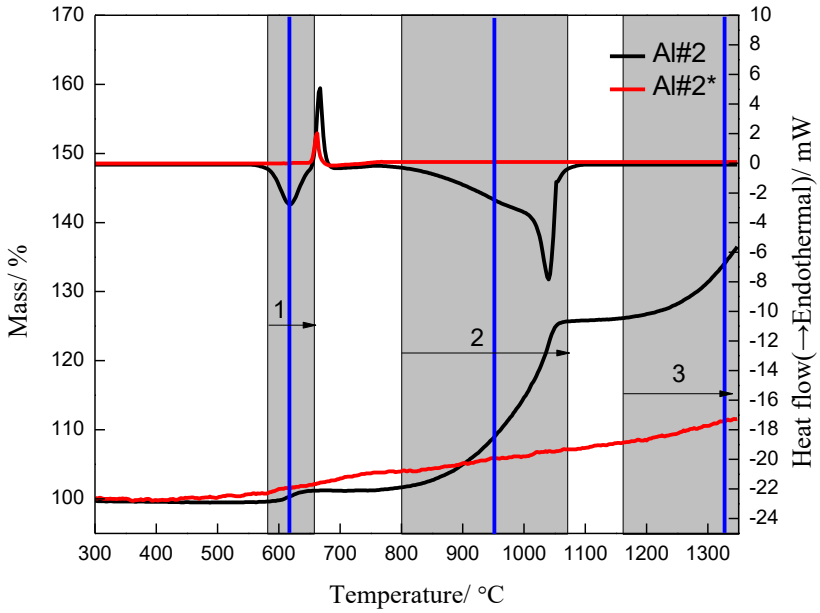

Figure 8: Comparison of TG-DSC Curves between Al#2 and Al#2*

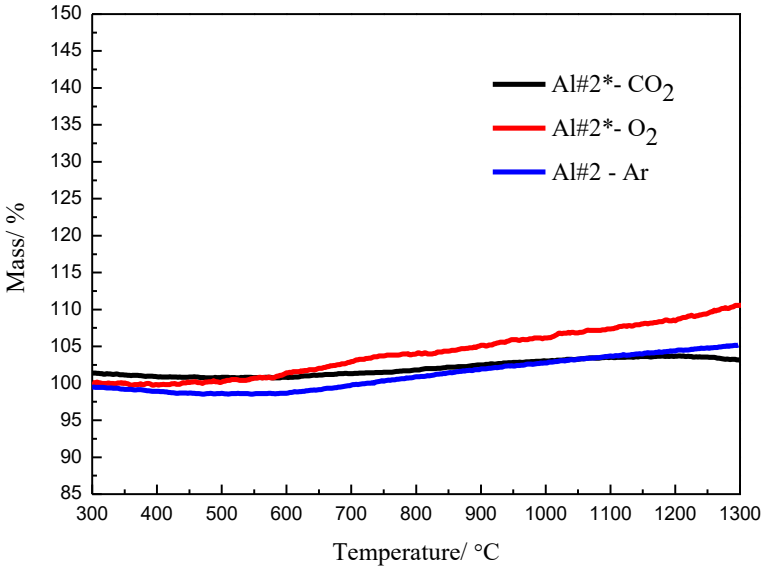

Figure 9: Comparison of TG-DSC Curves between Al#2 and Al#2*

4. Discussion

4.1. Slow Oxidation Mechanism of Micron Aluminum Powder

When heated to 650°C, the samples maintain a complete spherical state. The environmental oxygen reacts with the active aluminum, forming Al2O3 at the interface between the Al2O3 layer and active aluminum, increasing the thickness of the oxidation layer and resulting in weight gain. However, the degree

of oxidation is limited due to the intact oxide layer. When the temperature exceeds the melting point of aluminum, i.e., at the beginning of the second stage of weight increase at 950°C, the reaction products show a hollow shell structure and fragments of the Al2O3 shell. Al2O3 and Al have different coefficients of thermal expansion; the latter is 3-4 times that of the former. During heating, complex mechanical changes occur at the interface between Al and Al2O3 [26]. The expansion and phase transformation of the Al core apply pressure on the Al2O3 shell, and the liquefaction of the Al core intensifies expansion and diffusion. When internal pressure reaches a certain level, the Al shell disintegrates at the weak points of the Al2O3 layer, allowing molten aluminum to overflow and react with oxygen, leading to an explosive shelling reaction. The reaction mechanism is illustrated in Figure 10.

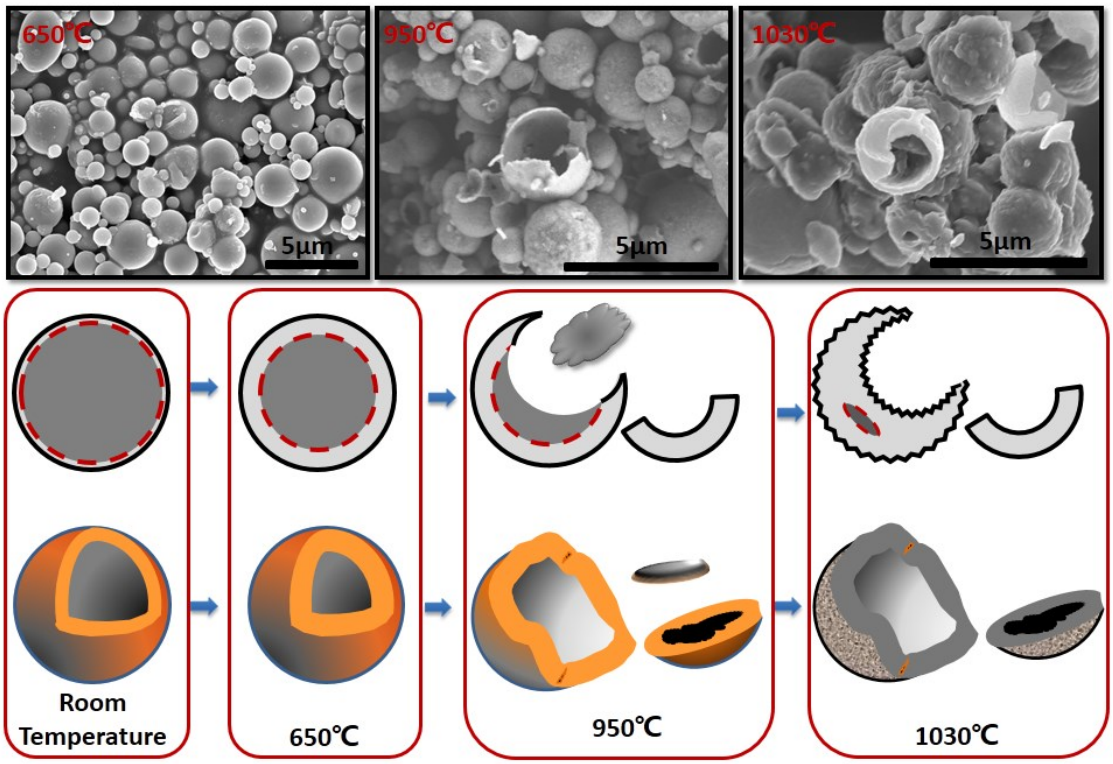

Figure 10: Mechanism of Aluminum Powders in Gradually Heated Process

4.2. Thermal Enhancement Mechanism of Micron Aluminum Powder Oxide Layer

γ-Al2O3 has a higher crystal density than amorphous Al2O3 (Table 3). After the thermal transformation of the aluminum powder oxide layer, the volume decreases, reducing the density. The environmental oxygen reacts with the internal liquid aluminum, forming Al2O3 at the interface, enhancing the oxide layer. After thermal enhancement, the internal aluminum of the high-temperature samples does not break the shell and react with the environmental oxidizing gases.

Table 3: Density and CTE of Aluminum and Different Phase of Alumina

Different phase of alumina	Density, g/cm3	CTE, k-1
Al	2.7	23.2*10-6(20℃)
Amorphous Al2O3	3-3.1	5.6-11*10-6
γ-Al2O3	3.6-3.67	(20-1400℃)
θ-Al2O3	3.4-3.9	
α-Al2O3	3.99	

Note: CTE is coefficient of thermal expansion

Calculating the relationship between the activity of alumina and the thickness of the oxide layer for the core-shell structure, the following assumptions are made:

1. Micron aluminum powder follows a log-normal distribution.
2. The thickness of the oxide layer for a sample is the set average value, disregarding the impact of particle size distribution.
3. Micron aluminum powder is a core-shell structure with good sphericity and uniform shell thickness.
4. Impurities are assumed to exist entirely within the aluminum core.

The active aluminum content of the original samples is obtained from Table 1. The mass and volume relationship is established using the densities of the aluminum core and alumina. The thickness of the oxide layer is derived from geometric relations, yielding the following calculation formula:

$$\bar{\delta} = \frac{d}{2} \cdot \left(1 - \sqrt[3]{\frac{Aa \cdot \rho_2}{Aa\ (\rho_2 - \rho_1) + \rho_1}}\right) \tag{3.2}$$

Where Aa (Active Aluminum) is the active aluminum content, d is the median particle size D50, ρ1 is the density of aluminum at 2.7g/cm3, and ρ2 is the density of alumina at 3.98 g/cm3.

For the enhancement process of the oxide layer, the change in the active aluminum content and oxide layer thickness is calculated based on the weight increase in the first stage of the reaction. The core-shell structure model presented in Figure 11 leads to the following assumptions:

1. The reaction interface is on the inside of the spherical oxide layer.
2. The reaction products are alumina and uniformly adhere to the internal oxide layer.
3. The spherical shell is rigid and does not deform during heating.

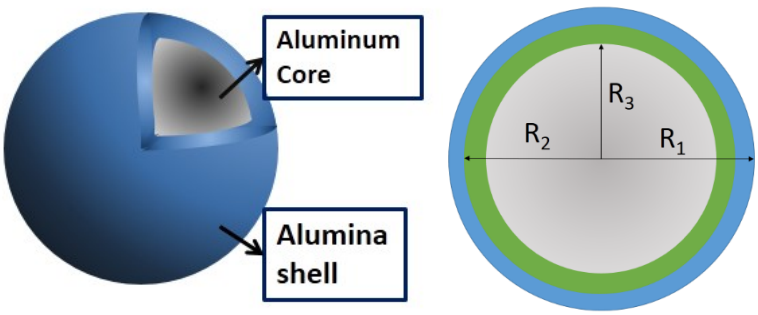

Figure 11: Core-shell Structure of Aluminum Powder

Equations 1 and 2 are derived from the reaction equation and the geometric structure of the aluminum powder, where W is the original mass of the sample particle, R1 is the original diameter, R2 is the inner diameter of the alumina shell, R3 is the inner diameter of the alumina shell after the first stage reaction, m is the weight increase obtained from the TG curve, ρ1 is the density of aluminum, and ρ2 is the density of alumina.

$$m = \frac{24}{51} \cdot \frac{4}{3}\pi\left(R_2^3 - R_3^3\right)\rho_2 \tag{3}$$

$$W = \frac{4}{3}\pi\left(R_1^3 - R_3^3\right)\rho_2 + \frac{4}{3}\pi R_2^3\rho_1 \tag{4}$$

Based on the formula, the calculation results for the thickness of the oxide layer before the first stage of heating and after heating at 620°C are as follows:

$$\delta_2 \geq 2\delta_1 \tag{5}$$

After the enhancement of the oxide layer, its thickness becomes twice the original thickness. When the thickness of the oxide layer is twice the original thickness, the slow heating reaction of micron aluminum powder is inhibited, preventing further oxidation reactions and leading to the deactivation of the aluminum powder.

5. Conclusion

The reaction of micron aluminum powder is divided into the following stages: from room temperature to 650°C, the phase transition of the oxide layer from amorphous to γ-phase, simultaneously increasing the thickness of the oxide layer to twice its original thickness under oxidation conditions, constituting thermal enhancement; upon reaching 670°C, the aluminum core melts, and the oxide layer undergoes stress effects with increasing temperature. As the temperature continues to rise to 950°C, the core-shell structure of micron aluminum powder breaks, allowing the internal active aluminum to contact the oxidizing atmosphere, resulting in an intense oxidation reaction, the main reaction stage; after 1150°C, micron aluminum powder continues to oxidize, while the original alumina and product alumina undergo high-temperature phase transitions, eventually forming α-phase alumina. The slow heating response process of the used micron aluminum powder particles follows an "explosive shelling" model.

The thermal enhancement of the micron aluminum powder oxide layer, i.e., slow heating in an oxidizing environment to 650°C, leads to the phase transition of the oxide layer to γ-alumina. First, the density reduces, causing a limited oxidation reaction between the oxidizing atmosphere and the active component, forming γ-alumina with the same thickness as the original layer, thereby restoring the density. Changes in the crystal structure and oxide layer thickness inhibit the slow heating process of micron aluminum powder, preventing the sample from undergoing slow oxidation reactions, resulting in complete deactivation under slow heating conditions.

6. Reference

[1] Dreizin E L, Schoenitz M. Correlating ignition mechanisms of aluminum-based reactive materials with thermoanalytical measurements. Progress in Energy & Combustion Science, 2015, 50:81-105.

[2] Starik A M, Savel'Ev A M, Titova N S. Specific features of ignition and combustion of composite fuels containing aluminum nanoparticles (Review). Combustion, Explosion, and Shock Waves, 2015, 51(2):197-222.

[3] Sundaram D S, Yang V, Zarko V E. Combustion of nano aluminum particles (Review). Combustion, Explosion, and Shock Waves, 2015, 51(2):173-196.

[4] Maggi F, Dossi S, Paravan C, et al. Activated aluminum powders for space propulsion. Powder Technology, 2015, 270:46-52.

[5] Li Ying, Song Wulin, Xie Changsheng, et al. Progress in the Application of Nano Aluminum Powder in Solid Propellants. ACTA ARMAMENTARII, 2005, 26(1):121-125.

[6] An Ting, Zhao Fengqi, Yi Jianhua, et al. Preparation, Characterization, Decomposition Mechanism and Non-Isothermal Decomposition Reaction Kinetics of the Super Thermite Al/CuO Precursor. ACTA PHYSICO-CHIMICA SINICA, 2011, 27(2): 281-288.

[7] Zhu Yan-Li, Jiao Qing-Jie, Huang Hao, et al. Effect of Aluminum Particle Size on Thermal Decomposition of AP. CHEMICAL JOURNAL OF CHINESE UNIVERSITIES, 2013, 34(3): 662-667.

[8] Zeng Liang, Jiao Qing-jie, Ren Hui, Zhou Qing. Effect of Particle Size of Nano-aluminum Powder on Oxide Film Thickness and Active Aluminum Content. Chinese Journal of Explosives & Propellants, 2011(4):26-29.

[9] Li Xin, Zhao Fengqi, Hao Haixia, et al. Research on Ignition and Combustion Properties of Different Micro/nano-aluminum Powders. Acta Armamentarii, 2014, 35(5):640-647.

[10] Puri P. Multi scale modeling of ignition and combustion of micro and nano aluminum particles. The Pennsylvania State University: Dissertations & Theses - Gradworks, 2008.

[11] Zhu X, Schoenitz M, Dreizin E L. Aluminum Powder Oxidation in CO2 and Mixed CO2/O2 Environments. Journal of Physical Chemistry C, 2009, 113(16):6768-6773.

[12] Badiola C, Gill R J, Dreizin E L. Combustion characteristics of micron-sized aluminum particles in oxygenated environments. Combustion & Flame, 2011, 158(10):2064-2070.
[13] Sippel T R, Pourpoint T L, Son S F. Combustion of Nanoaluminum and Water Propellants: Effect of Equivalence Ratio and Safety/Aging Characterization. Propellants Explosives Pyrotechnics, 2013, 38(1):56–66.
[14] Risha G A, Sabourin J L, Yang V, et al. Combustion and Conversion Efficiency of Nanoaluminum-Water Mixtures. Combustion Science and Technology, 2007, 180(12):2127-2142.
[15] Rossi S, Dreizin E L, Law C K. Combustion of Aluminum Particles in Carbon Dioxide. Combustion Science and Technology, 2001, 164(1):209-237.
[16] Ernst L F, Dryer F L, Yetter R A, et al. Aluminum droplet combustion in fluorine and mixed oxygen/fluorine containing environments. Proceedings of the Combustion Institute, 2000, 28(1):871–878.
[17] Gan Y, Li Q. Combustion characteristics of fuel droplets with addition of nano and micron-sized aluminum particles. Combustion & Flame, 2011, 158(2):354-368.
[18] Kong C, Dan Y, Qiang Y, et al. Morphological changes of nano-Al agglomerates during reaction and its effect on combustion. Combustion & Flame, 2016, 165:11-20.
[19] He Lirong, Xiao Leqin, Ding Haiqin, et al. TG-DSC research of shell's effect on activity of nano-aluminum powder. Ordnance Material Science and Engineering, 2013, 36(5): 21-25.
[20] Steenkiste T H V, Smith J R, Teets R E. Aluminum coatings via kinetic spray with relatively large powder particles. Surface & Coatings Technology, 2002, 154(2–3):237-252.
[21] Cheng Zhipeng, Yang Yi, Wang Yi, et al. Oxidation Ability of Nanocrystalline Ni-Coated Al Powders. ACTA PHYSICO-CHIMICA SINICA, 2008, 24(1):152-156.
[22] Zeng Liang. Core-shell Structure Aluminum Powder Impact on the Reaction Process of Aluminized Explosive. BEIJING: BEIJING INSTITUTE OF TECHNOLOGY, 2011:19-33.
[23] Zeng Liang, Jiao Qingjie, Ren Hui, et al. Studies on Oxide Film Thickness and Activity of Micron Aluminum Powder. Transactions of Beijing Institute of Technology, 2012, 32(2): 206-211.
[24] Rufino B, Boulc'H F, Coulet M V, et al. Influence of particles size on thermal properties of aluminium powder. Acta Materialia, 2007, 55(8):2815-2827.

7. Appendix

Supplementary Table: Parameters of Lognormal Fitting Curve

Parameter	Al#1	Al#2	Al#3	Al#4
y0	-0.29	-0.54	-0.51	-0.25
μ	2.56	6.31	15.15	29.67
σ	0.54	0.42	0.35	0.45
A	25.78	69.58	168.15	304.15
Correlation coefficient(%)	99.12	99.92	99.71	99.95